Colloid Polym Sci
DOI 10.1007/s00396-013-3159-7

ORIGINAL CONTRIBUTION

Structural insights on nanoparticles containing gadolinium complexes as potential theranostic

Antonella Accardo · Paola Ringhieri · Noemi Szekely · Vitaly Pipich · Alessandra Luchini · Luigi Paduano · Diego Tesauro

Received: 18 November 2013 / Revised: 23 December 2013 / Accepted: 29 December 2013

Abstract Nanostructures are gaining interest in drug release applications. Amphiphilic molecules can give, in water solution, a variety of nanostructures as well as thermodynamically stable mesophases three-dimensional inverse cubic structures. These mesophases are attractive candidates for biomedical applications containing extensive water channel networks and could act as very efficient delivery systems of drugs or contrast agents. In order to discover, optimize, and develop these systems, we have performed a deep physicochemical characterization by dynamic light scattering and small-angle neutron scattering of nanoparticles of monoolein (MO) and Pluronic PF127, containing different amounts (1, 5, 10, and 20 %) of the synthetic amphiphilic gadolinium complex $(C18)_2$DTPA(Gd). Nanoparticle size is found in the 70–400 nm range for all investigated systems; the morphology of the aggregates is driven by the main constituents MO/PF127 and is a mixture of multilayer vesicles and bicontinuous aggregates. Nanostructures are also able to encapsulate doxorubicin (drug-loading content between 70 and 90 % for the different systems) acting as a potential theranostic for simultaneous cancer therapy and MRI visualization.

A. Accardo · P. Ringhieri · D. Tesauro (✉)
CIRPeB, Department of Pharmacy & IBB CNR, University of Naples "Federico II", Via Mezzocannone, 16 80134 Naples, Italy
e-mail: dtesauro@unina.it

A. Luchini · L. Paduano (✉)
Department of Chemical Sciences, University of Naples "Federico II", Complesso Universitario di M.S. Angelo, Via Cinthia, 80126 Naples, Italy
e-mail: luigi.paduano@unina.it

N. Szekely · V. Pipich
Jülich Centre for Neutron Science, Garching Forschungszentrum, Lichtenbergstrasse 1, 85747 Garching bei München, Germany

Published online: 18 January 2014

Keywords Gadolinium contrast agent · Nanostructures · SANS study, oleins · MRI · Drug delivery

Introduction

Nanoscopic (10–500 nm) systems such as polymeric micelles, dendrimers, liposomes, and inorganic nanoparticles that incorporate therapeutic agents, diagnostic probes, and molecules for selective targeting are emerging as the next generation of multifunctional nanomedicines for improving the therapeutic outcome of drug therapy [1]. The motivations for the widespread of nanomedicine depend from the potential advantages of nanosystems with respect to conventional small molecule-based therapy: high payload capacity, reduced toxicity to healthy tissue, and improved antitumor efficacy [2–4]. The term "theranostic" was recently coined to describe multifunctional compounds able to combine diagnostic (PET and SPECT in combination with CT and/or MRI) and therapeutic modalities in one unified material, providing the chance to develop individually designed therapies against various diseases to accomplish personalized medicine [5]. Supramolecular aggregates containing Gd(III) complexes have been recently proposed as MRI contrast agents [6–9]. Liposomes, obtained by self-assembling aggregation of lipophilic gadolinium complexes or by their co-aggregation with surfactants, and micelles, based on amphiphilic poly(gadolinium complexes) polymers [10], display higher contrast efficacy with respect to MRI contrast agent based on isolated gadolinium complexes and peculiar pharmacokinetic properties. Moreover, gadolinium-based supramolecular aggregates could be easily derivatized with bioactive targeting molecules, such as peptides [8, 11–15] and antibodies [16–19]. These complex structures have been recently proposed as target selective MRI

contrast agents. Amphiphilic molecules could also aggregate in water solution, giving a variety of higher order two (2D)- or three-dimensional (3D) mesophases. Phases such as the 2D inverse hexagonal or the 3D inverse cubic structures are thermodynamically stable in water, and they can be dispersed as stable submicron-sized particles [20]. The nanostructures formed by dispersion of the bulk mesophases can offer substantial advantages with respect to traditional supramolecular aggregates; in fact they present: (a) much higher payloads of gadolinium ions compared to micellar and liposomal systems, (b) an expected increased relaxivity rate (1/T1) due to the slowing of the tumbling rate of the paramagnetic ions within the dense and highly ordered packing in the two- and three-dimensional networks of the hexagonal and cubic phases, and (c) improved relaxivity values due to the presence of extensive nanoscale water channels that offer a better environment for diffusion and fast exchange between gadolinium-coordinated water and bulk water. Contrast agents based on lanthanide complexes in highly ordered two- or three-dimensional mesophases have been initially proposed by Drummond et al. [21–25]. Recently, we reported on the preparation, structural characterization, and relaxometric behavior of new gadolinium-based contrast agents obtained by co-aggregation of an amphiphilic gadolinium complex, $(C18)_2$DTPA(Gd), with molar excesses of monoolein (MO) or diolein (DO) (Fig. 1) [26]. The obtained nanostructures display high relaxivity values and interesting relaxometric properties. We used monoolein and diolein in the nanostructure preparation for their known ability in giving highly ordered two- or three-dimensional mesophases in aqueous solution; anyway, the presence of the gadolinium-containing monomer seems to produce a partial loss of the cubic symmetry.

These nanostructures are gaining interest also for their potential application in controlled release and drug delivery. The bicontinuous water and oil channels, in aggregates such as cubosomes [27], allow for simultaneous incorporation of hydrophilic and hydrophobic active principles. Moreover, the pore structure provides a tortuous diffusion pathway for controlled release [28]. Several formulations for oral, transdermal, and systemic drug delivery have been recently proposed [29]. Here, we report a deep structural characterization by dynamic light scattering (DLS) and small-angle neutron scattering (SANS) of MO-based nanostructures doped with different amounts (1, 5, 10, and 20 %) of the synthetic amphiphilic gadolinium complex $(C18)_2$DTPA(Gd) (Table 1). The goal of these characterizations have two aims: determine the incidence of other aggregates like vesicles have two aims could substituted with are in these preparations and outline the best conditions for the obtainment of well-defined and stable highly ordered three-dimensional mesophases potentially acting as highly efficient MRI contrast agents. Moreover, drug loading of the anticancer doxorubicin (Dox) in monoolein-based nanostructures was also investigated for potential theranostic applications.

Experimental

Materials

Monoolein (1-monooleoyl glycerol, MO) was purchased by Sigma and had a purity of the acyl group (oleyl group) >99 % and a purity of the ester (monoglyceride) >97 %. A tri-block copolymer, containing ethylene oxide (EO) and propylene oxide (PO) groups, with the trade name Pluronic F127 (PF127) and an approximate formula of $EO_{98}PO_{57}EO_{98}$ (average molecular weight of 12,600 g mol^{-1}) was obtained from BASF Svenska AB (Helsingborg, Sweden). $(C_{18}H_{37})_2NCO(CH_2)_2COLys(DTPA)CONH_2$, [$(C18)_2$DTPA], was synthesized by solid-phase methods and purified by precipitation as previously described [30]. UV–vis measurements were performed on a UV–vis Jasco V-5505 spectrophotometer (Easton, MD) equipped with a Jasco

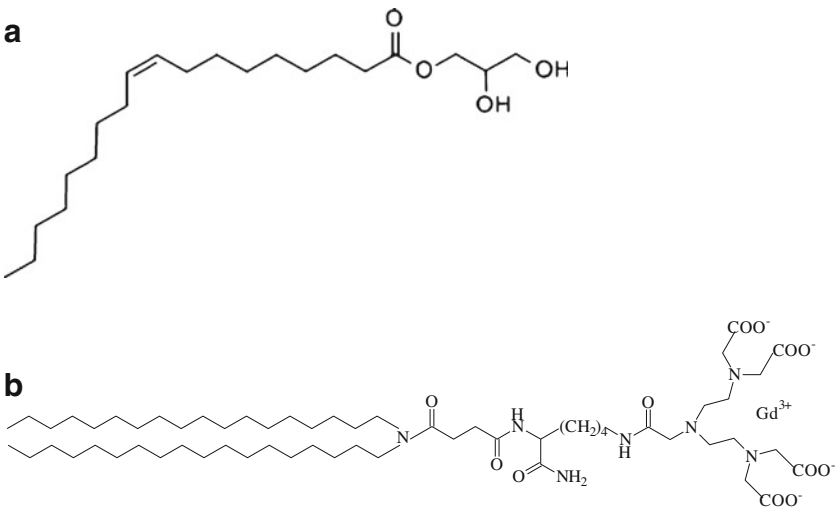

Fig. 1 Schematic representation of the commercially available monoolein (**a**) and of $(C_{18}H_{37})_2NCO(CH_2)_2COLys(DTPA\text{-}Gd)CONH_2$ [$(C18)_2$DTPA(Gd)] monomer (**b**)

Table 1 Composition (weight/weight percentage and molal concentration) of nanostructures based on MO

Samples	Composition %wt	Weight/weight percentage of Gd-DTPA$(C18)_2$	[MO]/mmol kg^{-1}	[Gd]/mmol kg^{-1}
A1	MO/D_2O	–	60.10	–
A2	MO/$(C18)_2$DTPA(Gd)/D_2O	1	57.10	0.16
A3	MO/$(C18)_2$DTPA(Gd)/D_2O	5	54.80	0.83
A4	MO/$(C18)_2$DTPA(Gd)/D_2O	10	50.30	1.58
A5	MO/$(C18)_2$DTPA(Gd)/D_2O	20	46.20	3.21

ETC-505 T Peltier temperature controller with a 1-cm quartz cuvette (Hellma).

Synthesis of nanostructures

Aqueous dispersions of MO (MO-NPs) containing various amounts of $(C18)_2$DTPA(Gd) amphiphilic gadolinium complex (1÷20 %) were prepared by the method previously described (the list of nanoaggregates are reported in Table 1) [26]. Briefly, MO, PF127, and $(C18)_2$DTPA(Gd) were weighed and mixed in chloroform. The weight ratio of PF127 to MO was 15 % (*w*/*w*). After evaporation of the solvent, the mixture was further dried in a vacuum. A 0.1 M phosphate buffer at pH 7.4 was added to the dry film, and the vials were immediately sealed and vortexed for several seconds to distribute water inside the samples. The mixture was sonicated in a bath sonicator for 30 min and left overnight under stirring. Finally, solutions were homogenized by ULTRA-TURRAX®(IKA® T18 basic) for 15 min in ice at 2.5 Hz.

Doxorubicin loading

Doxorubicin was remote-loaded in pure MO and in mixed MO/$(C18)_2$DTPA-Gd nanostructures (1÷20 molar ratios) by using the ammonium sulfate gradient method [31]. Briefly, nanostructure suspension (98/2 *w*/*w* H_2O/MO) was prepared as above reported in an ammonium sulfate solution (250 mM) at pH 5.5. After preparation, nanostructures were eluted on a Sephadex G-50 column pre-equilibrated with HEPES buffer (10 mM) at pH 7.4 and then incubated with an aqueous solution of Dox (3 mg/0.5 mL). The drug loading was studied at several g_{Drug}/g_{Lipid} ratios (0.05÷0.20). The suspension was stirred for 30 min at 60 °C, and subsequently, unloaded Dox was removed by gel filtration on a Sephadex column. The Dox concentration in all experiments was determined by UV–vis spectroscopy using calibration curves obtained by measuring absorbance at λ=480 nm. The drug-loading content (DLC; defined as the weight ratio of encapsulated Dox versus the olein forming nanostructures) was quantified by subtraction of the amount of removed Dox from the total amount of loaded Dox.

Physicochemical characterization

Dynamic light scattering

DLS measurements were performed with a homemade instrument composed by a Photocor compact goniometer, an SMD 6000 Laser Quantum 50 mW light source operating at 5,325 Å, a photomultiplier (PMT-120-OP/B), and a correlator (Flex02-01D) from *Correlator.com.* All measurements were performed at (25.00±0.05 °C) with temperature controlled through the use of a thermostat bath. In DLS, the intensity autocorrelation function $g^{(2)}(t)$ is measured and related to the electric field autocorrelation function $g^{(1)}(t)$ by the Siegert relation. This latter function can be written as the inverse Laplace transform of the distribution of the relaxation rate Γ used to calculate the translational diffusion coefficient $D=\Gamma/q^2$:

$$g^{(1)}(t) = \int_{-\infty}^{+\infty} \tau A(\tau) \exp\left(-\frac{t}{\tau}\right) \mathrm{d}\ln\tau \tag{1}$$

where $\tau=1/\Gamma$ and q is the modulus of the scattering vector $q=4\pi n_0/\lambda\sin(\theta/2)$, n_0 is the refractive index of the solution, λ is the incident wavelength, and θ represents the scattering angle. Laplace transforms were performed using a variation of CONTIN algorithm incorporated in Precision Deconvolve software. From Laplace transform, the average of the diffusion coefficient $\langle D\rangle$ and the diffusive polydispersity $i_D=\langle D^2\rangle/\langle D\rangle^2$ were obtained.

For spheres diffusing in a continuum medium at infinite dilution, the diffusion coefficient D_∞ is dependent on the sphere radius R_H, called *hydrodynamic radius*, through the Stokes–Einstein equation:

$$R_H = \frac{kT}{6\pi\eta_0 D_\infty} \tag{2}$$

where k is the Boltzmann constant, T is the absolute temperature, and η_0 is the solvent viscosity. For not spherical particles, R_H represents the radius of equivalent spherical

aggregates. Due to the high dilution, it is possible to make the approximation: $D \cong D_\infty$ and $\eta \cong \eta_0$, where η represents the solution viscosity. In this hypothesis, Eq. (2) can be reasonably used to estimate the hydrodynamic radius of the aggregates [32].

Small-angle neutron scattering

SANS measurements were performed at 25 °C with the KWS2 instrument located at the Heinz Meier-Leibtnitz Source, Garching Forschungszentrum (Germany). Neutrons with a wavelength spread $\Delta\lambda/\lambda \leq 0.2$ were used. A two-dimensional array detector at three different wavelength (W)/collimation (C)/sample-to-detector (D) distance combinations ($W_{7Å}C_{8m}D_{2m}$, $W_{7Å}C_{8m}D_{8m}$, and $W_{19Å}C_{8m}D_{8m}$), measured neutrons scattered from the samples. These configurations allowed collecting data in a range of the scattering vector modulus $q = 4\pi/\lambda \sin(\theta/2)$ between 0.0019 and 0.179 $Å^{-1}$, with θ scattering angle. The investigated systems were contained in a closed quartz cell in order to prevent the solvent evaporation and kept under measurement for a period sufficient to have ~2 million counts. Measurements at very small angle were performed at KWS3 running on the focusing mirror principle at the Research Neutron Source Heinz Maier-Leibnitz (FRM-II) in Garching. Standard configuration of the instrument with 9.5 m sample-to-detector distances allows performing scattering experiments with a wave vector transfer resolution between 10^{-4} and $3 \cdot 10^{-3}$ $Å^{-1}$, bridging a gap between Bonse–Hart and pinhole cameras. Second sample position at 1.3 m distances has extended Q-range of the instrument to $2 \cdot 10^{-2}$ $Å^{-1}$ and reached more than one-decade overlapping with the classical pinehole SANS instruments. The principle of this instrument is a one-to-one image of an entrance aperture onto a 2D position-sensitive detector by neutron reflection from a double-focusing toroidal mirror. The raw data were then corrected for background and empty cell scattering. Detector efficiency correction, radial average, and transformation to absolute scattering cross sections $d\Sigma/d\Omega$ were made with a secondary plexiglass standard [33, 34].

For a system composed by a collection of monodisperse bodies, the scattering cross section $d\Sigma/d\Omega$, that contains information on their interactions, sizes, and shapes, can be expressed as

$$\frac{d\Sigma}{d\Omega} = n_p P(q) S(q) + \left(\frac{d\Sigma}{d\Omega}\right)_{\text{incoh}} \quad (3)$$

where n_p represents the number density of the scattering objects in the system, $P(q)$ and $S(q)$ are the form and the structure factors of the scattering particles respectively, whereas $(d\Sigma/d\Omega)_{\text{incoh}}$ takes into account the incoherent scattering contribution, mainly due to the presence of hydrogen atoms. The form factor contains information on the shape of the scattering objects, whereas the structure factor accounts for interparticle correlation and is normally important for concentrated or charged systems. Structural parameters of the aggregates have been obtained by applying the appropriate models to the experimental SANS data as described in the "Results and discussion."

Results and discussion

Nanoparticles (NPs) of MO containing different amounts of $(C18)_2$DTPA(Gd) amphiphilic gadolinium complex (1, 5, 10, and 20 %) (Table 1) were formulated as previously reported [26]. Pluronic F127 in a 15 % *w*/*w* was also added to the nanoparticle composition; this surfactant acts as stabilizer of submicron particles with the bicontinuous cubic phase. All MO formulations showed high relaxivity values per Gd complex ($r_{1p} \approx 11$ mM^{-1} s^{-1} at 20 MHz and 298 K). These values did not change in a significant way by changing the Gd(III) complex content from 1 to 20 % in the nanostructures [26].

The physicochemical characterization has been carried out through dynamic light scattering and small-angle neutron scattering. In particular, dynamic light scattering data reveal the presence of a single broad distribution of aggregates in all the samples investigated, as shown in Fig. 2. The hydrodynamic radii R_H for all the systems, reported in Table 2, are located in the range of 70–400 nm. Furthermore, a large polydispersity is observed for all the analyzed systems being i_D ranged between 1.2 and 1.3 for the samples containing $(C18)_2$DTPA-Gd . We note that there is a marked difference in the polydispersity of the systems containing the gadolinium with respect to that formed by pure MO/PF127. This observation seems to suggest that the presence of charged moleculesrepresented by complex, (C18)2DTPA-Gd, does not affect the average sizes of the aggregates but instead produce a reduction of the polydispersity that in turn reflects in a descrease in the width of the radius distribution [35].

The morphology of these aggregates, as well as their geometrical characteristics, has been obtained by means of SANS measurements. Scattering cross sections for all the studied systems are reported in Fig. 3. Examination of the figure shows the presence, in the low q region, of a power law $(d\Sigma/d\Omega) \propto q^{-\alpha}$ where α is an exponent ranged between 2 and 4. These values are characteristic of systems containing multilamellar aggregates, being the exponent α strictly connected to the mean lamellarity of the supramolecular structure. In the limit case of $\alpha = 2$, the presence of unilamellar vesicles occurs. According to the phase diagram at the concentration studied, the MO/PF127 should form bicontinuous aggregates.

Indeed, the decay of the scattering profile for all the analyzed systems show a −3 power law at intermediate q values

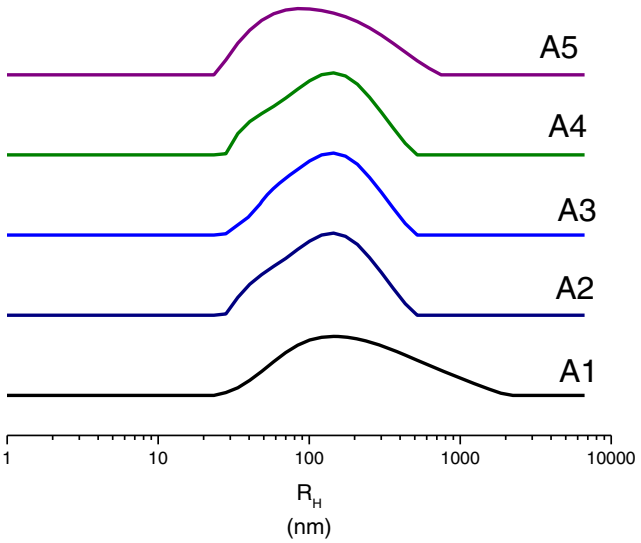

Fig. 2 Example of the hydrodynamic radii distribution at 90° of the aggregates present in the systems analyzed. For all the systems, the concentration was 0.2 mmol kg^{-1}

(0.004<q<0.015 Å), suggesting a complex structure of the aggregates as expected for systems containing bicontinuous aggregates. Furthermore, the scattering profiles observed for the samples A2, A3, A4, and A5 (i.e., those containing increasing amount of $(C18)_2$DTPA-Gd) are quite similar to that observed for the system A1 constituted by the pure MO/PF127 for which bicontinuous aggregates are expected [36].

Because of such evidences, the scattering profile obtained by SANS measurements has been modeled as a stack of lamellae. Under these hypothesis, the theoretical expressions of $d\Sigma/d\Omega$ is:

$$\frac{d\Sigma}{d\Omega}(q) = \frac{1}{q^2}\left\langle |f(q)|^2 \right\rangle \left(1 + \frac{\langle |f(q)| \rangle^2}{\left\langle |f(q)|^2 \right\rangle}(S(q)-1)\right) + \left(\frac{d\Sigma}{d\Omega}\right)_{incoh} \quad (4)$$

where $f(q)$ is the form factor of a bilayer containing information on the shape of the scattering objects, whereas $S(q)$ is the structure factor that takes into account the interferences occurring among the bilayers belonging to a single stack [37, 38].

Table 2 Mean characteristic physicochemical parameters obtained for the analyzed systems

Sample	<R_H>(nm)	i_D	τ(nm)	N	d(nm)	σ_d
A1	176±5	1.3	2.8±0.1	12±1	9.2±1.0	0.7±0.1
A2	144±4	1.1	2.8±0.2	14±2	5.4±0.7	0.6±0.1
A3	146±4	1.2	3.0±0.1	12±1	4.5±0.5	0.7±0.1
A4	140±5	1.2	3.0±0.2	11±3	6.3±0.8	0.6±0.1
A5	142±5	1.1	3.4±0.1	12±2	5.7±0.8	0.6±0.1

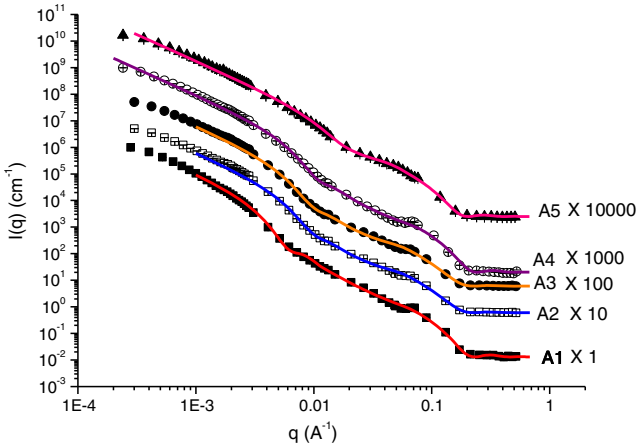

Fig. 3 Neutron scattering profiles of the studied systems. *Lines* correspond to the fitting equations as reported in the text. For a better visualization, data have been multiplied for a scale factor indicated in the plot

Finally, $(d\Sigma/d\Omega)_{incoh}$ represents the incoherent contribution to the cross section measured, mainly due to the presence of hydrogenated molecules.

From $d\Sigma/d\Omega$ experimental data vs. q several structural parameters can be optimized by a fitting procedure, namely: the number of layers in the stack, N, the mean layer thickness, τ, and the distance between the centers of two consecutive layers d. Actually, the number of layers N is generally only approximately determined; it gives rise to the upturn in scattering intensity at low q values where the total thickness of the stack is seen. In the adopted model, the polydispersity of τ and d is also admitted: for the former parameter, a Schulz–Zimm distribution function related to the Zimm polydispersity index Z is used, while for the latter one d, a Gaussian distribution with a standard deviation σ_d was preferred. As shown in figure, the model succeeds to predict the shape of the scattering profiles and the structural parameter extract from the fits are reported in Table 2.

It is worth noting that the pure MO/PF127 nanoaggregates exhibit a larger value of both hydrodynamic radius and distance between the centers of two consecutive layers d with respect to the systems in the presence of Gd complex. It likely that in the former system, there is a coexistence of multilamellar aggregates (larger size) and cubosomes (smaller size) and that upon addition of $(C18)_2$DTPA-Gd, the vesicles reorganize in cubosome [26, 39].

In conclusion from the structural point of view, the physicochemical characterization suggests that the cubosome can be lodge a considerable amount of amphiphilic contrast agent without that this latter destabilizes the bicontinuous structure.

The drug-loading capability of monoolein-based nanostructures was also investigated. Dox encapsulation into the nanostructures was carried out by using the sulfate ammonium gradient method previously performed in anionic-chelating-containing liposomes [40]. The other method (namely the pH method) largely employed for the doxorubicin loading was

not pursuable because of the poor solubility of nanostructures at pH 4.0. In particular, nanostructures containing high percentage of gadolinium complexes, in which the head group presents a COO^- group, show very low solubility and thus precipitate. DLC of pure monoolein was 95 % at drug/lipid (*w*/*w*) ratio of 0.15. When the amount of the $(C18)_2$DTPA-Gd increases in the nanostructure, the DLC slowly decreases until 70 % for the mixed nanostructures containing 20 % of the gadolinium complex. A DLC of 95 % was obtained by performing the doxorubicin encapsulation at drug/lipid (*w*/*w*) ratio of 0.10.

Conclusion

A deep structural characterization of nanoaggregates based on monoolein and Pluronic PF127 containing different amounts of the amphiphilic Gd complex is necessary to define the external and internal structures of the cubic mesophases. The amphiphilic Gd complex containing aggregates shows the same morphology of the pure MO/PF127 aggregates up to 20 % in mole of $(C18)_2$DTPA-Gd. This suggests that the size and shape of the aggregates are mainly derived by these two components and that the amphiphilic contrast agent can be introduced in the formulation without any loss in the aggregates structure. The bicontinous aggregates show a size of 14 nm, a thickness of the bilayers of about 3 nm with a mean distance between the centers of the layers of about 5 nm.

Relaxometric properties, size, and shape of the nanostructure as well the doxorubicin-loading ability suggest that the obtained nanocompounds could act as theranostics for simultaneous cancer therapy and MRI visualization.

Acknowledgments This work was supported by grants from the Italian Minister of Research (MIUR): grant FIRB RBRN07BMCT, grant PRIN E61J11000300001, and grant PRIN 2009235JB7. The Italian Consortium CIRCMSB is also gratefully acknowledged. Some of the authors (N.S.,V.P., A.L., and L.P.) thank the Julich Centre for Neutron Science for provision of beam time. SANS experiments were supported by the European Commission, NMI3.

References

1. Accardo A, Tesauro D, Morelli G (2013) Peptide-based targeting strategies for simultaneous imaging and therapy with nanovectors. Polym J 45:481–494
2. Park K, Lee S, Kang E, Kim K, Choi K, Kwon IC (2009) New generation of multifunctional nanoparticles for cancer imaging and therapy. Adv Funct Mater 19:1553–1566
3. Simeone L, Mangiapia G, Vitiello G, Irace C, Colonna A, Ortona O, Montesarchio D, Paduano L (2012) Cholesterol-based nucleolipid-ruthenium complex stabilized by lipid aggregates for antineoplastic therapy. Bioconjugate Chem 23:758–770
4. Mangiapia G, D'Errico G, Simeone L, Irace C, Radulescu A, Di Pascale A, Colonna A, Montesarchio D, Paduano L (2012) Ruthenium-based complex nanocarriers for cancer therapy. Biomaterials 33:3770–3782
5. Thakare VS, Das M, Jain AK, Patil S, Jain S (2010) Carbon nanotubes in cancer theragnosis. Nanomedicine 5:1277–1301
6. Delli Castelli D, Gianolio E, Geninatti Crich S, Terreno E, Aime S (2008) Metal containing nanosized systems for MR-molecular imaging applications. Coord Chem Rev 252:2424–2443
7. Mulder WJM, Strijkers GJ, Van Tilborg GAF, Cormode DP, Fayad ZA, Nicolay K (2009) Nanoparticulate assemblies of amphiphiles and diagnostically active materials for multimodality imaging. Acc Chem Res 42:904–914
8. Accardo A, Tesauro D, Aloj L, Pedone C, Morelli G (2009) Supramolecular aggregates containing lipophilic Gd(III) complexes as contrast agents in MRI. Coord Chem Rev 253(17–18):2193–2213
9. Mulder WJM, Strijkers GJ, van Tilborg GAF, Griffioen AW, Nicolay K (2006) Lipid-based nanoparticles for contrast-enhanced MRI and molecular imaging. NMR Biomed 19(1):142–164
10. Tesauro D, Accardo A, Gianolio E, Paduano L, Texeira J, Schillen K, Aime S, Morelli G (2007) Peptide derivatized lamellar aggregates as target specific MRI contrast agents. ChemBioChem 8:950–955
11. van Tilborg GAF, Mulder WJM, Deckers N, Storm G, Reutelingsperger CPM, Strijkers GJ, Nicolay K (2006) Annexin A5-functionalized bimodal lipid-based contrast agents for the detection of apoptosis. Bioconjugate Chem 17:741–749
12. Mulder WJM, van der Schaft DWJ, Hautvast PAI, Strijkers GJ, Koning GA, Storm G, Mayo KH, Griffioen AW, Nicolay K (2007) Early in vivo assessment of angiostatic therapy efficacy by molecular MRI. FASEB J 21(2):378–383
13. Brandwijk RJMGE, Mulder WJM, Nicolay K, Mayo KH, Thijssen VLJL, Griffioen AW (2007) Anginex-conjugated liposomes for targeting of angiogenic endothelial cells. Bioconjugate Chem 18: 785–790
14. Vaccaro M, Mangiapia G, Paduano L, Gianolio E, Accardo A, Tesauro D, Morelli G (2007) Structural and relaxometric characterization of peptide aggregates containing gadolinium complexes as potential selective contrast agents in MRI. ChemPhysChem 8: 2526–2538
15. Morisco A, Accardo A, Gianolio E, Tesauro D, Benedetti E, Morelli G (2009) Micelles derivatized with octreotide as potential target-selective contrast agents in MRI. J Pept Sci 15:242–250
16. Mulder WJM, Strijkers GJ, Griffioen AW, van Bloois L, Molema G, Storm G, Koning G, Nicolay K (2004) A liposomal system for contrast-enhanced magnetic resonance imaging of molecular targets. Bioconjugate Chem 15:799–806
17. Mulder WJM, Strijkers GJ, Briley-Saebo KC, Frias JC, Aguinado JGS, Vudic E, Amirbekian V, Tang C, Chin PTK, Nicolay K, Fayad ZA (2007) Molecular imaging of macrophages in atherosclerotic plaques using bimodal PEG-micelles. Magn Reson Med 58(6): 1164–1170
18. Lipinski MJ, Amirbekian V, Frias JC, Aguinado JGS, Mani V, Briley-Saebo KC, Fuster V, Fallon JT, Fisher EA, Fayad ZA (2006) MRI to detect atherosclerosis with gadolinium-containing immunomicelles targeting the macrophage scavenger receptor. Magn Reson Med 56(3):601–610
19. Amirbekian V, Lipinski MJ, Briley-Saebo KC, Amirbekian S, Aguinado JGS, Weinreb DB, Vucic E, Frias JC, Hyafil F, Mani V, Fisher EA, Fayad ZA (2007) Detecting and assessing macrophages in vivo to evalute atherosclerosis noninvasively using molecular MRI. Proc Natl Acad Sci U S A 104(3):961–966
20. Yaghmur A, Glatter O (2009) Characterization and potential applications of nanostructured aqueous dispersions. Adv in Colloid Interface Sci 147–148:333–342
21. Liu G, Conn CE, Waddington LJ, Mudie ST, Drummond CJ (2010) Colloidal amphiphile self-assembly particles composed of gadolinium oleate and myverol: evaluation as contrast agents for magnetic resonance imaging. Langmuir 26(4):2383–2391

22. Liu G, Conn CE, Drummond CJ (2009) Lanthanide oleates: chelation, self-assembly, and exemplification of ordered nanostructured colloidal contrast agents for medical imaging. J Phys Chem B 113:15949–15959
23. Conn CE, Panchagnula V, Weerawardena A, Waddington LJ, Kennedy DF, Drummond CJ (2010) Lanthanide phytanates. Liquid-crystalline phase behavior, colloidal particle dispersions, and potential as medical imaging agents. Langmuir 26(9):6240–6249
24. Moghaddam MJ, de Campo L, Waddington LJ, Weerawardena A, Kirby N, Drummond CJ (2011) Chelating oleyl-EDTA amphiphiles: self-assembly, colloidal particles, complexation with paramagnetic metal ions and promise as magnetic resonance imaging contrast agents. Soft Matter 7:10994–11005
25. Moghaddam MJ, de Campo L, Waddington LJ, Drummond CJ (2010) Chelating phytanyl-EDTA amphiphiles. Self-assembly and promise as contrast agents for medical imaging. Soft Matter 6:5915–5929
26. Accardo A, Gianolio E, Arena F, Barnert S, Schubert R, Tesauro D, Morelli G (2013) Nanostructures based on monoolein or diolein and amphiphilic gadolinium complexes as MRI contrast agents. J Mater Chem B 1:617–628
27. Shah JC, Sadhale Y, Chilukuri DM (2001) Cubic phase gels as drug delivery systems. Adv Drug Deliv Rev 25:229–250
28. Anderson DM, Wennerström H (1990) Self-diffusion in bicontinuous cubic phases, L3 phases, and microemulsions. J Phys Chem 94: 8683–8694
29. Kogan A, Garti N (2006) Microemulsions as transdermal drug delivery vehicles. Adv Colloid Interface Sci 123–126:369–385
30. Accardo A, Morisco A, Gianolio E, Tesauro D, Mangiapia G, Radulescu A, Brandt S, Morelli G (2011) Nanoparticles containing octreotide peptides and gadolinium complexes for MRI applications. J Pept Sci 17:154–162
31. Fritze A, Hens F, Kimpfler A, Schubert R, Peschka-Süss R (2006) Remote loading of doxorubicin into liposomes driven by a transmembrane phosphate gradient. BBA Biomembranes 1758: 1633–1640
32. Vergara A, Paduano L, Sartorio R (2001) Multicomponent diffusion in systems containing molecules of different size. 4. Mutual diffusion in the ternary system tetra(ethylene glycol)-di(ethylene glycol)-water. J Phys Chem B 105:328–334
33. Wignall GD, Bates FS (1987) Absolute calibration of small-angle neutron scattering data. J Appl Crystallogr 20:28–40
34. Russell TP, Lin JS, Spooner S, Wignall GD (1988) Inter- and absolute calibration of SAXS and SANS data. J Appl Crystallogr 21:629–638
35. Vaccaro M, Mangiapia G, Radulescu A, Schillén K, D'Errico G, Morelli G, Paduano L (2009) Colloidal particles composed of amphiphilic molecules binding gadolinium complexes and peptides as tumor-specific contrast agents in MRI: physico-chemical characterization. Soft Matter 5:2504–2512
36. Gustafsson J, Ljusberg-Wahren H, Almgren M, Larsson K (1997) Submicron particles of reversed lipid phases in water stabilized by anonionic amphiphilic polymer. Langmuir 13:6964–6971
37. Vaccaro M, Del Litto R, Mangiapia G, Carnerup AM, D'Errico G, Ruffo F, Paduano L (2009) Lipid based nanovectors containing ruthenium complexes: a potential route in cancer therapy. Chem Commun 1404–1406
38. Frielinghaus H (2007) Physical review E. Stat Nonlinear Soft Matter Phys 76:051603/051601–051603/051608
39. Mangiapia G, Vaccaro M, D'Errico G, Frielinghaus H, Radulescu A, Pipich V, Carnerup AM, Paduano L (2011) Cubosomes for ruthenium complex delivery: formulation and characterization. Soft Matter 7:10577–10580
40. Morisco A, Accardo A, Tesauro D, Palumbo R, Benedetti E, Morelli G (2011) Peptide labeled supramolecular aggregates as selective doxorubicin carriers for delivery to tumor cells. Biopolymers Pept Sci 86:88–96